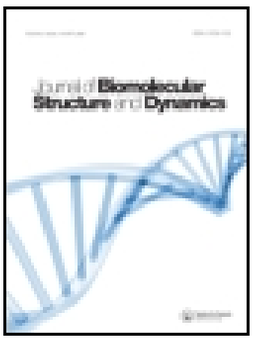

Taylor & Francis
Taylor & Francis Group

Journal of Biomolecular Structure and Dynamics

ISSN: (Print) (Online) Journal homepage: https://www.tandfonline.com/loi/tbsd20

Drug repurposing for Alzheimer's disease: *in silico* and *in vitro* investigation of FDA-approved drugs as acetylcholinesterase inhibitors

Navneet Kumar , Anuj Gahlawat , Rajaram Naresh Kumar , Yash Pal Singh , Gyan Modi & Prabha Garg

To cite this article: Navneet Kumar , Anuj Gahlawat , Rajaram Naresh Kumar , Yash Pal Singh , Gyan Modi & Prabha Garg (2020): Drug repurposing for Alzheimer's disease: *in silico* and *in vitro* investigation of FDA-approved drugs as acetylcholinesterase inhibitors, Journal of Biomolecular Structure and Dynamics, DOI: 10.1080/07391102.2020.1844054

To link to this article: https://doi.org/10.1080/07391102.2020.1844054

JOURNAL OF BIOMOLECULAR STRUCTURE AND DYNAMICS
https://doi.org/10.1080/07391102.2020.1844054

Drug repurposing for Alzheimer's disease: *in silico* and *in vitro* investigation of FDA-approved drugs as acetylcholinesterase inhibitors

Navneet Kumar[a], Anuj Gahlawat[a], Rajaram Naresh Kumar[a], Yash Pal Singh[b], Gyan Modi[b] and Prabha Garg[a]

[a]Department of Pharmacoinformatics, National Institute of Pharmaceutical Education and Research (NIPER), S.A.S. Nagar, Mohali, Punjab, India; [b]Department of Pharmaceutical Engineering & Technology, Indian Institute of Technology (Banaras Hindu University), Varanasi, Uttar Pradesh, India

Communicated by Ramaswamy H. Sarma

ABSTRACT

Alzheimer's disease (AD) is one of the most familiar multifactorial and complex neurodegenerative disorders characterized by loss of cholinergic neurons in the brain. The various attempts for drug development to treat AD have been hampered by largely unsuccessful clinical trials in the last two decades. Developing a new drug from scratch takes enormous amounts of time, effort and money, mainly due to several barriers in the therapeutic drug development process. Drug repurposing strategy resuscitates this slow drug discovery process by finding new uses and clinical indications for existing drugs. This study is focused on the cholinergic hypothesis, a well-established target of the clinically available drugs in the market for the treatment of AD. The computational virtual screening (VS) led to the identification of thiazolidinedione (TZD, antidiabetic) and aminoquinoline (antimalarial) class of drugs as acetylcholinesterase (AChE) inhibitors. Intriguingly, rosiglitazone (RGZ) and hydroxychloroquine (HCQ) were found to be mild-to-moderate inhibitors of *h*AChE (human acetylcholinesterase) in our enzyme inhibition studies which are complementary to our computational studies. On the basis of our computational and experimental studies, it can be suggested that the beneficial effect of RGZ and HCQ in AD patients reported in the literature may partly be due to their AChE inhibitory property. The VS also led to the identification of antifungal drugs miconazole and oxiconazole as potential AChE inhibitors. The molecular dynamics (MD) simulation of the potential hits belonging to TZD, aminoquinoline and azoles class were also carried out. The MD simulations studies revealed detailed computational insights related to molecular interactions and protein–ligand stability for selected hits.

ARTICLE HISTORY
Received 19 June 2020
Accepted 23 October 2020

KEYWORDS
Alzheimer's disease; drug repurposing; hydroxychloroquine; rosiglitazone; MD simulations; virtual screening

CONTACT Prabha Garg prabhagarg@niper.ac.in Department of Pharmacoinformatics, National Institute of Pharmaceutical Education & Research (NIPER), Sector-67, S.A.S. Nagar, Mohali, Punjab-160062, India

Supplemental data for this article can be accessed online at https://doi.org/10.1080/07391102.2020.1844054

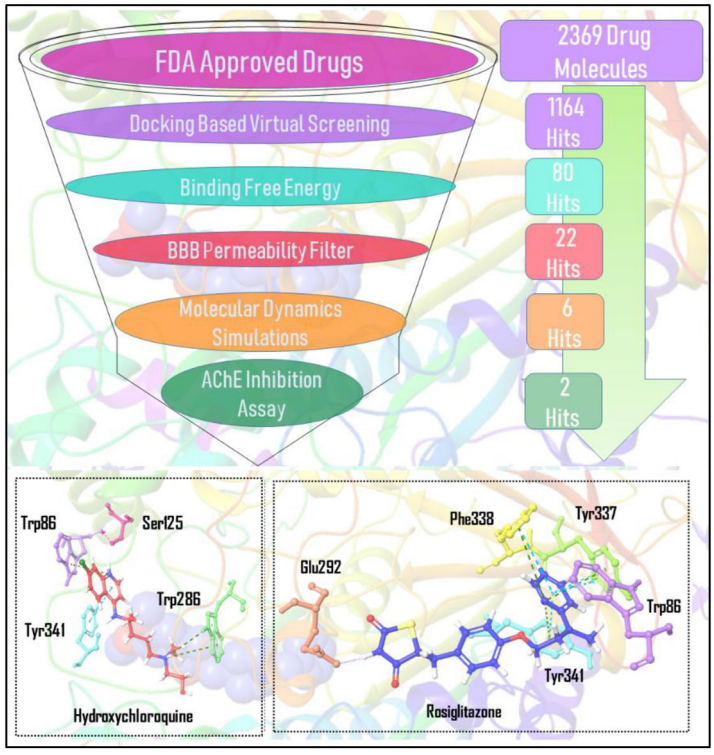

Abbreviations: AD: Alzheimer's disease; ACh: acetylcholine; AChE: acetylcholinesterase; DZP: donepezil; RGZ: rosiglitazone; PIO: pioglitazone; HCQ: hydroxychloroquine; MCZ: miconazole; OXZ: oxiconazole; TZD: thiazolidinedione; T2DM: type 2 diabetes mellitus

1. Introduction

Alzheimer's disease (AD) is a progressive neurodegenerative disorder leading to impairment in memory, language skills, personal behavior and thinking. The exact pathogenesis and etiology of this progressive disorder are still dubious (Burns & Iliffe, 2009; Mayeux & Stern, 2012). However, there are several hypotheses that help in explaining the plausible reasons for the onset of the disease. The amyloid and τ-protein aggregation hypotheses include deposition of various species of amyloid β and τ-proteins in the dying neurons (Castro & Martinez, 2006; Grundke-Iqbal et al., 1986; Kumar, Ganeshpurkar, et al., 2018; Kumar, Gupta, et al., 2018), cholinergic hypothesis supports the diminished level of neurotransmitter especially acetylcholine (ACh, Gauthier et al., 2005; Holzgrabe et al., 2007), metal dyshomeostasis (Ayton et al., 2015; Singh et al., 2019) and oxidative stress (Scarpini et al., 2003) also play an important role in the pathophysiology of this disease. All these hypotheses tend to provide the potential targets to treat AD. Among all these hypotheses, the cholinergic pathway remains one of the promising targets for the treatment of AD. Acetylcholinesterase (AChE) is an enzyme belonging to the carboxylesterase family, catalyzes the hydrolysis of excess ACh into acetic acid and choline after neurotransmissions (Francis et al., 1999). The cholinergic hypothesis refers to the selective decreased level of ACh in the brain which is caused by an enhanced activity of AChE in AD and old age. Therefore, the currently available treatments for AD in the market including donepezil (DZP), rivastigmine and galantamine are well-known AChE inhibitors (Colovic et al., 2013; McGleenon et al., 1999; Mehta et al., 2012). These inhibitors work by slowing the process of degradation of ACh which increases both the level and duration of the neurotransmitter.

Drug repurposing is a sub-branch of polypharmacology which deals with marketed or withdrawn drugs, as their pharmacokinetic and safety profile are already known in the human population. This approach is implemented to scrutinize other new clinical indications for marketed drugs. It overcomes cost, time and risk of failure during the drug development process. It also helps in dose adjustment of a drug against a target while keeping minimal effect on other known targets. Different experimental and computational approaches have been used to frame these multiple target interactions of drugs, to avoid side effects and to design rational drugs for disease. Computational methods are fast, less expensive and can easily handle large datasets as compared to experimental methods (Karaman & Sippl, 2019; Pushpakom et al., 2019; Talevi & Bellera, 2020). There are various drug molecules that have been successfully repurposed for other targets. The phosphodiesterase-5 inhibitor, sildenafil, an erectile dysfunction drug has been indicated for cardiovascular disorders indications (Raja & Nayak, 2004). Procainamide (local anesthetic), hydralazine

(antihypertensive) and olsalazine (anti-inflammatory) were repurposed for epigenetic activity on DNA methyltransferase (Méndez-Lucio et al., 2014). There are many other drugs like thalidomide (withdrawn due to teratogenesis), ketoconazole (antifungal), itraconazole (antifungal), acrisorcin (antifungal) and mebendazole (antihelminthic) were repurposed for new disease indications multiple myeloma, Cushing's syndrome, angiogenesis inhibitor, antimalarial and cancer, respectively (Naveja et al., 2016).

It has been reported in the literature that various marketed drugs which were indicated for different diseases like cancer, diabetes, depression, heart and epilepsy also have an affinity toward various targets of AD and these typical drugs include carmustine (anticancer) (Hayes et al., 2013), lisinopril (ACE [angiotensin-converting enzyme] inhibitor) (Singh et al., 2013), telmisartan (angiotensin receptor blockers) (Singh et al., 2013), divalproex sodium (antiepileptic) (Tariot et al., 2011), levetiracetam (antiepileptic) (Sanchez et al., 2012), tetracycline (antibacterial) (Forloni et al., 2001), minocycline, nilvadipine (calcium channel blocker) (Meulenbroek et al., 2016; Ryu et al., 2004), perindopril (ACE inhibitor) (Dong et al., 2011), rosiglitazone (RGZ, antidiabetic) (Miller et al., 2011), rasagiline (anti-Parkinson) and liraglutide (antidiabetic) (Hughes et al., 2016). Bansode et al. carried out drug repurposing via docking and biophysical assay on 140 centrally acting FDA-approved drugs and reported multiple targets (i.e. AChE, β-secretase and amyloid β aggregation) for protriptyline (antidepressant) to treat AD (Bansode et al., 2014). Similarly, Nousheen et al. explored the anti-Alzheimer mechanism of bexarotene (anticancer) using computational biology approach and found it impedance on amyloid β peptide aggregation (Bibi et al., 2019). Shivani et al. used docking-based approach to screen 150 antipsychotic drugs against BACE1 (beta-site amyloid precursor protein cleaving enzyme 1), BuChE (butyrylcholinesterase), AChE, MAO (monoamine oxidase) and NMDA (N-methyl-D-aspartate) as AD's targets and reported good potential for pimozide, bromperidol, benperidol, etc. (Kumar et al., 2017).

It is clear from the above discussion that drug repurposing offers a new solution to complex biological problems. Thus, in this study, a combination of computational and experimental approaches was utilized to identify FDA-approved drugs as potential AChE inhibitors. Amongst all the top hits identified, the thiazolidinedione (TZD) and aminoquinoline class of drugs were already reported to show mixed effects in AD patients (Aisen, 2002; Aisen et al., 2001; Pedersen et al., 2006; Pérez & Quintanilla, 2015). Earlier studies have also indicated AChE inhibition properties of chloroquine in μM range *in vitro* assays (Katewa & Katyare, 2005; Lim & Go, 1985). Our finding through virtual screening (VS) and *in vitro* studies indicates AChE inhibition property of HCQ of which could provide synergistic effects in addition to its reported anti-inflammatory property. Similarly, this study also elaborates on detailed computational insights on selected hits in terms of important molecular interactions, stability and binding mode using molecular dynamics (MD) simulations.

2. Materials and methods

2.1. Molecular docking

The 3 D crystal structure of *h*AChE (human acetylcholinesterase) in complex with DZP (PDB ID-4EY7) was retrieved from the Brookhaven protein data bank (Berman et al., 2000; Cheung et al., 2012). Protein Preparation Wizard of Schrödinger software package (Schrödinger, LLC, New York, NY) was used to prepare the protein. This step includes addition of missing hydrogen, removal of water beyond 5 Å from the HET group, assignment of right bond orders, optimization of orientations of hydroxyl and amino groups and the determination of ionization of amino acids using ProtAssign utility. The resulting structures were further subjected to restrained minimization with cutoff root mean square deviation (RMSD) of 0.3 Å. Finally, the prepared complex was further used for molecular docking and MD simulation study.

All the FDA-approved drugs obtained from the DrugBank database (Wishart et al., 2008) available at (https://www.drugbank.ca/) were subjected for ligand preparation using the LigPrep module of Schrödinger software package (Schrödinger, LLC, New York, NY). The different possible ionization states were generated at the pH (7.0 ± 2) using Epik ionizer.

The receptor grid generation module of Schrödinger software package (Schrödinger, LLC, New York, NY) was used to define the site of molecular docking. The grid center was defined using the centroid of co-crystallized ligand, i.e., DZP. The grid was standardized by re-docking the co-crystallized ligand DZP. Further, the docked ligand in the previous step was aligned to co-crystallized ligand to compare the RMSD value between them. Molecular docking of all ligands was performed in extra precision (XP) mode (Friesner et al., 2006).

2.2. Virtual screening protocol

A combined VS protocol was used to get the promising top hits from a list of FDA-approved drugs. It comprises molecular docking, Prime/MM-GBSA (molecular mechanics/generalized born surface area) calculation (Genheden & Ryde, 2015) and blood-brain barrier (BBB) permeability filter. DrugBank (Wishart et al., 2008) consists of a total of 2389 FDA-approved drugs. All ligands (FDA-approved drugs) were docked to AChE in XP mode using the method described in Section 2.1 or in our previous study (Arora et al., 2019). Docked molecules having XP GScore lower than −9.0 were further subjected to Prime/MM-GBSA calculation. All the poses of small molecules having different docking scores were considered during the MM-GBSA calculation. Finally, those molecules which have binding free energy lesser than the DZP were used in the next step of screening. The next stage of filtering was based on BBB permeability using the ADMET Descriptor module of Discovery Studio 2.5 software (Discovery Studio Visualizer 2.5.5 (2010) Accelrys Inc.) (Egan & Lauri, 2002). Few molecules were selected amongst the final top filtered molecules for MD simulations to assess the stability of docked complexes. Also, a detailed analysis of key interacting residues was performed during the whole period

of MD simulations for the selected ligands. Apart from this, a rigorous MM-GBSA calculation was performed on MD trajectory to estimate the average binding free energy of different protein–ligand complexes to remove any false positives obtained from VS protocol. Finally, two compounds were subjected to *in vitro h*AChE inhibition assay selected on the basis of the absence of experimental evidence reported in literature.

2.3. Molecular dynamics simulations

All-atom MD simulations were performed using the Desmond-v6.1 module (Bowers et al., 2006) of Schrödinger software package (Schrödinger, LLC, New York, NY). The system builder panel was used to prepare the initial system for MD simulations. Apo-AChE and all docked complexes were placed in a cubic box of 1.0 nm size. The box was solvated with TIP3P water models (Mark & Nilsson, 2001) and negative charge of the system was neutralized using Na^+ ions. An ionic strength of 0.15 M was maintained by adding Na^+ and Cl^- ions to the system. Further, the solvated system was minimized and equilibrated under NPT ensemble using the default protocol of Desmond. It includes a total of nine stages among which there are two minimization and four short simulations (equilibration phase) steps (Samad et al., 2016). All minimized and equilibrated systems were subjected to MD run with periodic boundary conditions in NPT ensemble using OPLS_2005 force field parameter (Shivakumar et al., 2010) for 100 ns. During the simulation, the pressure (1 atm) and temperature (300 K) of the system were maintained by Martyna–Tobias–Klein barostat and Nose–Hoover Chain thermostat, respectively (Cho et al., 1993; Evans & Holian, 1985; Hoover, 1985; Nosé, 1984). Binding energy between the AChE and all ligands was calculated using the inbuilt script thermal_mmgbsa.py (Genheden & Ryde, 2015; Lyne et al., 2006). An average of binding energy between protein and ligand was calculated from the last 30 ns of trajectory. The solvent accessibility surface area (SASA) of AChE in the presence of different ligands was calculated using the script binding_sasa.py. Apart from this, the number of hydrogen bonds were also calculated using the simulation event analysis panel and in-house codes.

2.4. In vitro hAChE inhibition assays

The inhibitory activity for ChE was performed using the modified method of Ellman et al. (1961) and following the previous work of Kumar, Ganeshpurkar, et al. (2018), Kumar, Gupta, et al. (2018) and Singh et al. (2020). Cholinesterase (ChE) catalyzes the hydrolysis of acetylthiocholine iodide (ATCI) to produce the thiocholine and acetate, which reduces the 5,5-dithiobis-(2-nitrobenzoic acid) (DTNB) to yellow color product that can be detected colorimetrically at 415 nm. *h*AChE (CAS No. 9000-81-1), DTNB (CAS No. 69-78-3), ATCI (CAS No. 1866-15-5), DZP (CAS No. 120011-70-3), hydroxychloroquine (HCQ, CAS No. 747-36-4) and RGZ (CAS No. 122320-73-4) were purchased from Sigma-Aldrich. The stock solution of enzyme 0.022 U/mL was prepared in a 50 mM Tris-HCl buffer (pH 8.0). DZP was used as a standard drug. The stock solutions of test and standard (2.5 mM) were prepared in molecular biology grade dimethyl sulfoxide (DMSO). The percentage inhibitions were determined at five different concentrations of 20, 10, 1.0, 0.1 and 0.01 μM of test compounds. Briefly, 50 μL of AChE (0.022 U mL^{-1}) and 10 μL of test or standard compounds were incubated in 96-well plates for 30 min at room temperature. Further, 30 μL (1.5 mM) of substrate ATCI were added into it and allowed to stand for an additional 30 min. Finally, 160 μL of DTNB (0.15 mM) was added to it, and absorbance was recorded immediately at 415 using Synergy HTX multi-mode reader (BioTek, USA). Results are expressed as the mean ± SEM of at least three different experiments performed in triplicate. The blank assay consisted of all components except enzyme and control contain all components except test compound. The percentage inhibition was calculated from the equation: $1-A_i/A_c \times 100$, where A_i and A_c are the absorbance values obtained for AChE in the presence and absence of inhibitors, respectively.

3. Results

3.1. Virtual screening

3.1.1. Molecular docking-based virtual screening

The crystal structure of AChE with co-crystallized ligand DZP was used for the molecular docking using the Glide in XP mode (Friesner et al., 2006). The co-crystallized ligand DZP was used to define the grid. The co-crystallized ligand was redocked to the AChE and the binding poses of both co-crystallized and redocked DZP were compared and the RMSD difference between them was found to be 0.657 Å (Supplementary Figure S1). The VS of all the 2389 FDA-approved drugs was performed using the same validated grid. All the molecules having XP GScore lesser than −9.0 kcal/mol were selected in order to have a diverse set of molecules for the next stage of screening.

3.1.2. Binding free energy calculation

Binding free energies of docked protein–ligand complexes were calculated using the Prime/MM-GBSA method. Combining the docking results with Prime/MM-GBSA not only rank a large set of ligands rapidly but also yield more reliable results and remove any false positives (Genheden & Ryde, 2015; Lyne et al., 2006). A cutoff of (XP GScore) −9.0 kcal/mol filter 1164 compounds out of a total of 2389 compounds from docking-based VS. The binding free energy of 1164 docked complexes was computed. A total of 80 compounds were predicted to have binding free energy lesser than the DZP. The predicted binding free energy of DZP bound to AChE was found to be −84.82 kcal/mol.

3.1.3. BBB permeability predictions

The BBB permeability is one of the imperative requirements for a drug molecule which is intended to target and treat AD. All 80 molecules screened in the previous step on the basis of binding free energy were further subjected to BBB

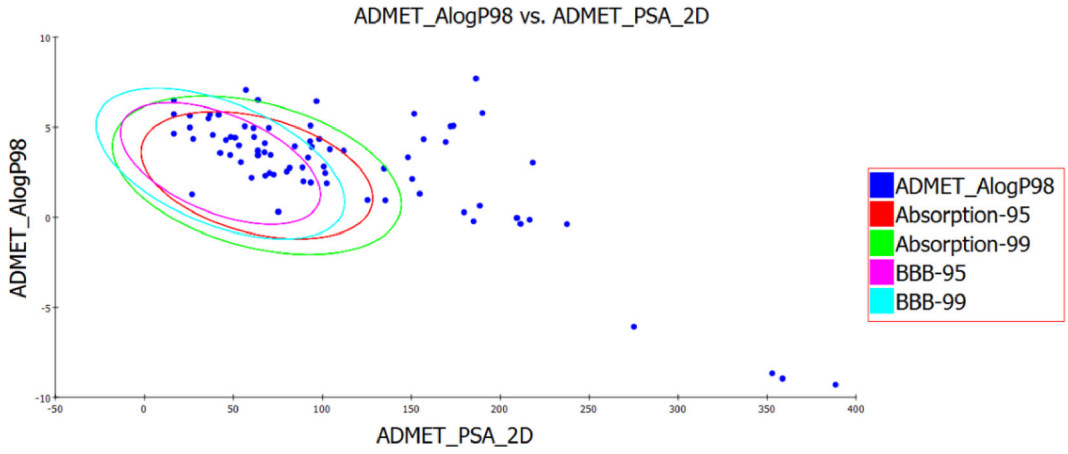

Figure 1. Plot of PSA versus AlogP for the 80 hits obtained from docking and free energy-based virtual screening method. The 95% and 99% confidence limit ellipses that correspond to the blood-brain barrier model.

permeability prediction. The ADMET Descriptor module of Discovery Studio 2.5 predicts the blood-brain penetration of small molecules after the oral administration. This method is based on quantitative linear regression which predicts the blood-brain penetration, as well as 95% and 99% confidence ellipses in the ADMET_AlogP98, ADMET_PSA_2D plane. There are four prediction levels within the 95% and 99% confidence ellipsoids. The different prediction level of molecules is identified by four different values, i.e., 0 (very high penetrant), 1 (high), 2 (medium), 3 (low) and 4 (undefined). In this study, only those molecules which are predicted to have very high or high penetrant represented by values 0 and 1 were considered. A total of 22 compounds were retained out of 80 compounds using BBB filter. Figure 1 shows the plot of PSA versus AlogP for the 80 hits obtained from docking and free energy-based VS method. Table 1 depicts the docking results, important interaction (hydrogen bond and hydrophobic interaction) between residues of AChE and small molecules, binding free energy and BBB prediction level of top 22 top hits.

Out of 22 compounds obtained from a combined computational VS method, top 10 molecules were considered for further study. A literature search was performed for top 10 molecules. It was found that RGZ and pioglitazone (PIO) belonging to TZD class of antidiabetic drugs which acts by activation of the peroxisome proliferator-activated receptor γ (PPAR-γ). Both drug molecules have been already shown to be therapeutically beneficial in mild-to-moderate stages of AD (Pedersen et al., 2006; Pérez & Quintanilla, 2015). Another aminoquinoline class of drugs including HCQ and piperaquine (PPQ) is mainly used in the treatment of malaria. Apart from antimalarial activity, HCQ is also a prescribed medication in the treatment of rheumatoid arthritis, chronic discoid lupus erythematosus and systemic lupus erythematosus (Al-Bari, 2015). Recently, HCQ in combination with azithromycin has been used in novel coronavirus (COVID-19) patients which is caused by infection of SARS-CoV-2 virus (Gautret et al., 2020). HCQ's ability to inhibit the destructive inflammatory mechanisms have shown benefit in AD (Aisen, 2002; Aisen et al., 2001). So, the antidiabetic drugs (RGZ and PIO) and antimalarial drug HCQ have shown to be beneficial in the treatment of AD but none of the mechanisms suggests anything related to cholinergic hypothesis. PPQ is a bisquinoline antimalarial drug which is also structurally related to HCQ. Since PPQ is ranked on top in *in silico* VS study and structural similarity of this molecule with HCQ led us to study this molecule in more detail along with other top hits. Miconazole (MCZ) and oxiconazole (OXZ) belonging to the imidazole family is used as antifungal agents have also shown good affinity for AChE in our computational study. In literature, only MCZ has been already reported to inhibit the AChE with 0.65 ± 016 μM (Chen et al., 2015). Since OXZ shares similarity in structure with MCZ and both belong to the same chemical class (imidazole derivative), we expect that OXZ should also show AChE inhibitory activity with almost similar potency as that of MCZ. We did not find any experimental evidence where the biological inhibitory activity of OXZ against *h*AChE is reported. The reported study on MCZ focuses very little on computational aspects so we included MCZ along with OXZ for MD simulation study.

Our next stage of study focused on identifying the structural stability, detailed interaction analysis of AChE with six selected molecules and average binding free energy calculation over a trajectory snapshot using MD simulations. Six hits, i.e., HCQ, PPQ, RGZ, PIO, MCZ, OXZ and reference molecule DZP in complex with AChE were selected for MD simulation study.

3.2. Molecular dynamics simulations

The MD simulation study of AChE_apo state and aforementioned hits along with reference crystallized molecule DZP in complex with AChE were carried out for 100 ns. This study further shed the light on the detailed computational insights in terms of molecular interactions, protein–ligand stability and binding modes for all six drug molecules.

3.2.1. Analysis of interaction of different drug molecules with AChE

3.2.1.1. Hydroxychloroquine and piperaquine. The quinoline moiety of HCQ interacts with the catalytic active site while the long chain having positive charged amine group

Table 1. Docking, binding free energy and BBB permeability results of top 22 molecules obtained from virtual screening of DrugBank database.

S. No.	Generic_name	glide gscore	glide emodel	Docking score	XP GScore	MM-GBSA dG bind	ADMET_ BBB_Level	Hydrogen bonding	π–π interaction	π–cation
1	Piperaquine	−18.24	−116.85	−17.98	−18.24	−125.3	0	Phe295	Trp286 His447	Trp86, Tyr341
2	Pipazethate	−14.64	−74.13	−12.33	−14.64	−97.50	1		Trp86	Trp86
3	Pioglitazone	−14.64	−87.50	−13.15	−14.64	−96.57	1	Ser293, Arg296, Tyr124	Tyr341,His447, Tyr337, Trp86	Trp86
4	Oxiconazole	−11.23	−94.02	−10.19	−11.23	−94.17	0	Ser125	Tyr337, His447, Trp286	
5	Miconazole	−11.93	−96.16	−11.72	−11.93	−93.36	0	Asp74, Tyr124	Trp86, Tyr124	
6	Nefazodone	−16.90	−117.23	−16.83	−16.90	−91.88	1	Phe295	Trp86	Trp86, Tyr337, Phe338
7	Abemaciclib	−14.22	−109.12	−11.57	−14.22	−91.65	1	Phe295, Tyr72	Trp286, Tyr341	Trp86
8	Rosiglitazone	−9.71	−78.48	−9.57	−9.71	−91.56	1	Phe295	Trp86, Tyr337 Tyr341	Phe338
9	Hydroxychloroquine	−12.09	−82.40	−12.04	−12.09	−91.03	1	Ser125, Arg296	Trp86	Trp286
10	Econazole	−11.49	−91.11	−11.29	−11.49	−91.00	0	Tyr124, Asp74	Trp86, Tyr124	
11	Sulconazole	−11.39	−91.98	−11.06	−11.39	−90.16	0	Asp74	Tyr124	
12	Isoconazole	−13.14	−84.64	−12.94	−13.14	−89.66	0	Tyr337	Trp286, His447, Tyr337	Trp86
13	Astemizole	−12.33	−97.29	−12.0	−12.33	−89.10	0	Tyr124	Trp286, Trp86	Tyr337, Trp86
14	Bifonazole	−13.20	−71.50	−12.87	−13.20	−89.09	0	His447	Phe338, Tyr341	Trp86
15	Terconazole	−9.46	−116.24	−9.21	−9.46	−88.81	1	Ser293	Tyr341	
16	Lapyrium	−10.97	−76.49	−10.97	−10.97	−88.81	1	Trp86		Trp86
17	Penbutolol	−9.47	−68.63	−9.47	−9.47	−87.95	1	Tyr124, His447	Tyr337, Phe338	Trp86
18	Mebeverine	−16.33	−101.42	−16.33	−16.33	−86.92	1	Phe338 Gly122	Trp286, His447	Phe338, Tyr337, Trp86
19	Drotaverine	−11.34	−83.40	−9.21	−11.34	−86.74	1		Tyr337, His447, Trp286	
20	Brexpiprazole	−13.41	−103.27	−13.28	−13.41	−86.67	1	Phe295	Trp286 Trp86	Tyr337, Phe338, Tyr341
21	Butoconazole	−10.85	−78.83	−10.47	−10.85	−86.66	0		Trp286 Trp86	
22	Chloroquine	−9.7	−68.15	−9.66	−9.7	−85.08	0	Tyr124	Tyr341	Trp86, Tyr341, Phe338
23	Donepezil	−17.50	−87.40	−17.48	−17.50	−84.82	1	Phe295	Trp286, Trp86	Phe338, Tyr337, Trp86

interacts with peripheral active site (PAS) of AChE. During the initial period of MD simulation, the interaction between the quinoline ring and Trp86 via π–π stacking was observed occasionally. While this same interaction (i.e. Trp86 and quinoline moiety) was found to be more prominent during the last 30 ns of simulation maintained via both π–π stacking and π–cation interaction (Figure 2). This π–cation interaction between Trp86 (belonging to catalytic anionic subsite or choline-binding subsite) and quaternary ammonium ligands is already reported to be important in the literature (Junaid et al., 2019; Santos et al., 2018; Zhang et al., 2018). Terminal quaternary nitrogen in the side chain also forms a π–cation interaction with Trp286 and this interaction with PAS was maintained for more than 50% of simulation time (Figure 3(C), Supplementary Figure S2(B)). The quinoline fragment of HCQ also makes hydrogen bonds with the residue Ser125 and since this interaction was maintained for 88% of total simulation time, it can be considered as one of the strong and consistent interactions (Figure 3(C), Supplementary Figure S2(B)). Other important and consistent interaction of HCQ with AChE includes a hydrogen bond between Tyr341 and amino group directly attached to quinoline at the fourth position. Supplementary Figures S4–S6 show interactions and contacts (H-bonds, Hydrophobic, Ionic, Water bridges) in timeline form. The timeline figure, having the top panel shows the total number of specific contacts the AChE makes with the HCQ over the course of the trajectory and the bottom panel shows residues and ligand interaction information in each trajectory frame. The residues making more than one specific contact with the ligand is represented by a darker shade of orange, according to the scale to the right of the plot.

PPQ belongs to the 4-aminoquinoline class having two quinoline groups joined by a linker which is composed of two piperazine moieties. One terminal quinoline moiety mainly orients toward the catalytic active site while the opposite quinoline moiety orients toward the PAS (Figure 3(B)). The PAS residue, i.e., Trp286 forms π–cation interaction with nitrogen of quinoline, and this interaction was maintained for 40% of total simulation time. Also, this residue forms π–π stacking with one ring of quinoline (Figure 3(B), Supplementary Figure S2(C)). Glu292 is another PAS residue which forms salt bridge and one hydrogen bond with this terminal quinoline group. The opposite quinoline moiety interacts mainly with Trp86 and Tyr449 via π–π stacking and π–cation interaction. The electron-rich π system of aromatic rings present in both amino acids, i.e., Trp86 and Tyr449 make strong and consistent π–cation interaction with the positive charged quaternary amine present in the quinoline group (Figure 3(B), Supplementary Figure S2(C)). MD simulation analysis on the basis of occupancy and histogram in Supplementary Figure S2(C) indicates that the interaction of PPQ with both PAS and catalytic site is stable and maintained throughout the simulation time.

3.2.1.2. Rosiglitazone and pioglitazone. RGZ is mainly composed of TZD rings attached to a lipophilic group through phenoxyalkyl linker. The TZD moiety of RGZ mainly interacts

with PAS and lipophilic tail (i.e., pyridine) interacts with catalytic site of AChE (Figure 4(B)). The TZD ring makes one hydrogen bond directly and one water-mediated hydrogen bond with Glu292, and this interaction was present in the majority of time during the whole period of simulation (Figure 4(B), Supplementary Figure S3(C)). The histogram depicts (Supplementary Figure S3(C)) hydrogen bond and water-mediated hydrogen bond (in two different colors) between Glu192 and TZD moiety of RGZ. The lipophilic pyridine moiety present at the terminal of RGZ mainly interacts with the residues of the catalytic anionic site of AChE.

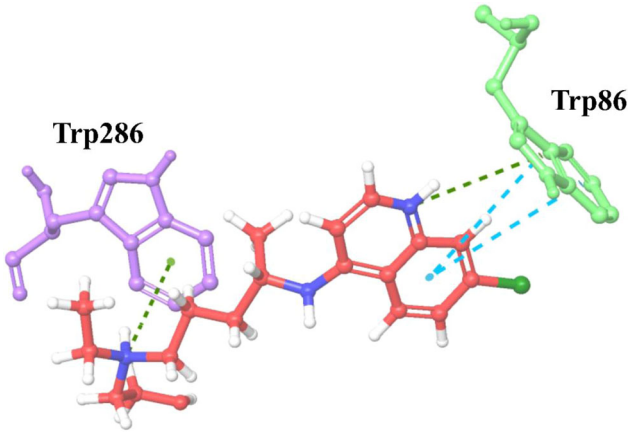

Figure 2. The π–π interaction (cyan color) and π–cation interaction (green color) between quinoline group of hydroxychloroquine and Trp86 consistent only during the last 30 ns of simulation, while the π–cation interaction (green color) between Trp286 and hydroxychloroquine was consistent during the whole simulation time.

Residues Trp86, Tyr337 and Tyr341 form π–π stacking with the pyridine ring and having occupancy of 46%, 60% and 49%, respectively. The nitrogen of pyridine interacts with residues Trp86, Tyr337, Phe338 and Tyr341 through the π–cation interaction. These π–cation interactions were maintained for more than 60% of total simulation time for all four residues (Supplementary Figure S3(C)). The residues Trp86 and Tyr337 are the important residues of catalytic anionic site of AChE and hydrophobic interactions with these residues for different potent ligands including DZP are reported in the literature.

Similar to RGZ, TZD moiety of PIO also interacts with PAS and tail part (i.e., pyridine) orient toward the catalytic site of AChE (Figure 4(A)). The positively charged amine group in TZD rings make two hydrogen bond with Glu292 and Gln291. Residue Glu292 also forms a water-mediated hydrogen bond with oxygen of TZD ring in a similar fashion to RGZ. The pyridine ring forms hydrophobic interaction with Tyr337 and Phe338. The timeline representation of interaction (Supplementary Figure S5(C)) and histogram (Supplementary Figure S3(D)) represents that important interacting residues belonging to both catalytic and PAS are stable and consistent.

3.2.1.3. Miconazole and oxiconazole. The imidazole ring present in MCZ interacts with PAS and one dichlorobenzene ring interacts with the catalytic site of AChE (Figure 3(D)). The nitrogen in the imidazole ring forms a water-mediated hydrogen bond with Asn87. This water-mediated hydrogen bond was maintained for more than 40% of total simulation

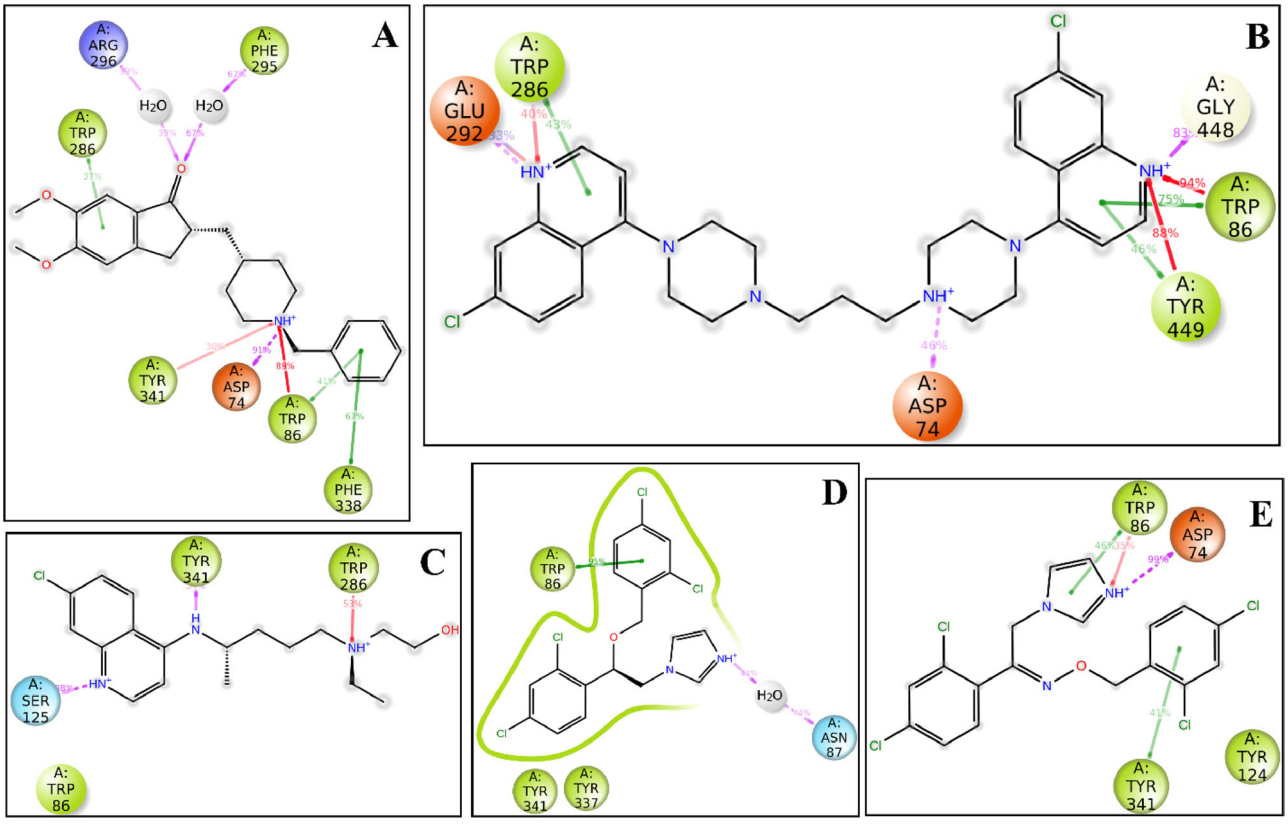

Figure 3. 2D interaction diagram of *h*AChE with (A) donepezil, (B) piperaquine, (C) hydroxychloroquine, (D) miconazole and (E) oxiconazole, where green, red and violet colored arrows represent the π–π stacking, π–cation interactions and hydrogen bonds, respectively.

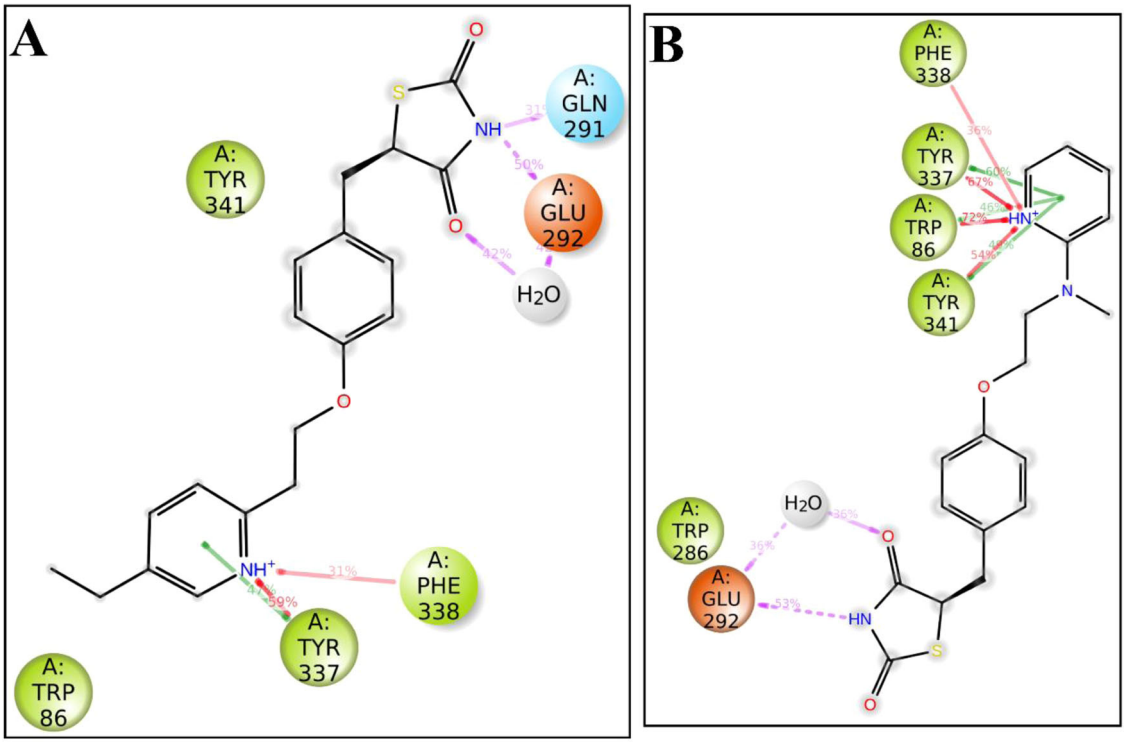

Figure 4. 2D interaction diagram of *h*AChE with (A) pioglitazone and (B) rosiglitazone where green, red and violet colored arrows represent the π–π stacking, π–cation interactions and hydrogen bonds, respectively.

time (Supplementary Figure S3(A)). Another important and stable hydrophobic interaction was observed between dichlorobenzyl ring and Trp86, and this π–π stacking interaction with anionic site residue was maintained over 95% of total simulation time (Figure 3(D), Supplementary Figure S3(A)).

It was observed that the dichlorobenzyl group of OXZ forms a π–π stacking with Trp86, and this hydrophobic interaction was maintained for only initial 20 ns of simulation. After 20 ns of simulation Trp86 form π–π stacking and π–cation stacking with the imidazole group of OXZ (Figure 5(A,B)). This is one of the important events observed during the MD simulations. Also, this same moiety forms a hydrogen bond with Asp74 (Figure 3(E), Supplementary Figure S3(B)). Imidazole ring of OXZ interacts with both catalytic sites and PAS of AChE.

3.2.2. Analysis of binding free energy

The binding free energy between the AChE and all seven ligands was calculated from the last 30 ns trajectory. The average binding free energy and its different contributing terms for all simulated complexes are summarized in Table 2. Figure 6 shows the fluctuation in the binding free energy of all complexes with respect to simulation time. The plot shows that binding free energy of all complexes with respect to time fluctuates around a stable value. The average binding energy of AChE_HCQ and AChE_PPQ complexes was found to be −84.64 ± 5.5 and −105.09 ± 7.7 kcal/mol, respectively. Similarly, the binding energy for both antifungal drugs MCZ and OXZ with AChE was found to be −81.77 ± 4.9 and −92.37 ± 4.6 kcal/mol, respectively. Remaining both TZD class of antidiabetic drugs, RGZ and PIO in complex with AChE were found to have almost equal average binding free energy of approximately −88 kcal/mol. The van der Waals energy remains one of the major contributing terms to final average binding energy for all complexes. The van der Waals energy contributed negatively to total binding energy for all complexes and the value for all complexes lies in a similar range. The coulombic energy is considered as another important energetic term which contributes to final binding energy between protein–ligand complexes. It was noted that similar to van der Waals energy, the coulombic energy also contributes negatively to total binding energy for all complexes except the TZD drug molecules RGZ and PIO.

3.2.3. Analysis of structural stability, compactness and residual fluctuation

The structural stability of AChE and its complex with different ligands can be explained by analyzing the RMSD, radius of gyration (R_g) and root mean square fluctuation (RMSF). Figure 7 shows the RMSD plot of apo-AChE and its complex with the different ligands. The changes in RMSD for all complexes suggest that the simulation is converged. This plot also suggests that binding of ligands causes a significant reduction in the RMSD value. The average RMSD values along with standard deviation were calculated for all complexes and were compared with apo-AChE (Supplementary Table S1). There is a considerable reduction in average RMSD value of AChE in the presence of all ligands. Figure 7 shows the changes in the R_g of the AChE in the presence and in absence of the ligands. The R_g is an indicator of the compactness of the protein. The R_g plot (Figure 8) and average

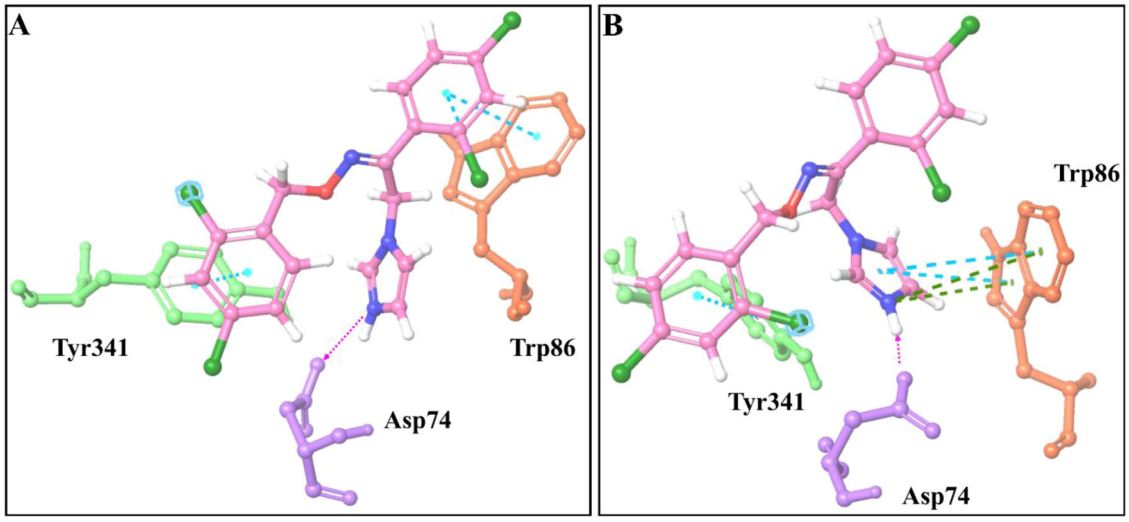

Figure 5. (A) interaction of Trp86 of *h*AChE with dichlorobenzyl group of oxiconazole during the first 20 ns of simulation and (B) interaction of Trp86 shifted to imidazole group from dichlorobenzyl group after 20 ns.

Table 2. The average ΔG_{bind} (kcal/mol) and its contributing energy terms for six hits against *h*AChE calculated from MD trajectories (last 30 ns).

Complex	Avg. ΔG_{bind} Coulomb[a]	Avg. ΔG_{bind} Covalent[b]	Avg. ΔG_{bind} Hbond[c]	Avg. ΔG_{bind} Lipo[d]	Avg. ΔG_{bind} Packing[e]	Avg. ΔG_{bind} solv GB[f]	Avg. ΔG_{bind} vdW[g]	ΔG_{bind} total[h]
AChE_DZP	−24.28	3.58	−0.82	−34.61	−3.98	43.41	−52.27	−68.96 ± 3.4
AChE_HCQ	−12.03	5.58	−2.09	−24.32	−8.46	4.16	−47.47	−84.64 ± 5.5
AChE_PPQ	−51.78	4.51	−1.18	−30.42	−14.96	49.51	−60.79	−105.09 ± 7.7
AChE_MCZ	−20.75	1.40	−0.16	−33.83	−6.17	30.61	−52.88	−81.77 ± 4.9
AChE_OXZ	−17.22	2.41	−0.76	−30.12	−5.06	10.06	−51.69	−92.37 ± 4.6
AChE_RGZ	11.69	4.82	−1.15	−30.97	−7.94	−18.61	−46.42	−88.57 ± 7.4
AChE_PIO	10.82	2.72	−0.79	−30.69	−6.07	−12.25	−51.80	−88.06 ± 4.6

[a]Coulomb energy,
[b]Covalent binding energy,
[c]Hydrogen bonding correction,
[d]Lipophilic energy,
[e]Pi–pi packing correction,
[f]Generalized born electrostatic solvation energy,
[g]van der Waals energy,
[h]Total binding free energy.

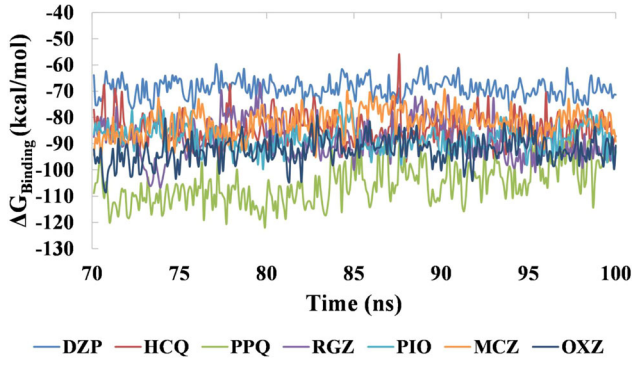

Figure 6. Binding free energy of AChE with donepezil, hydroxychloroquine, piperaquine, hydroxychloroquine, rosiglitazone, pioglitazone, miconazole and oxiconazole with respect to simulation time calculated using the MM-GBSA method from the last 30 ns of MD simulation.

R_g calculated from the whole trajectory (Supplementary Table S1) indicate that there are no considerable and significant changes in R_g of AChE in the presence of ligands as compared to apo-AChE. The RMSF locates the region of local residual fluctuation in AChE in the presence and absence of ligand. RMSF for AChE-apo state provides a baseline for comparing the fluctuations with ligand-bound complexes. One region from residues 71 to 95 (say region A) has a spike and comparatively higher RMSF value as compared to other regions in case of apo-AChE (Supplementary Figure S7). But it was observed that the binding of ligands stabilizes the spike region A. The binding of almost all ligands stabilizes the higher fluctuations in this region including standard drug molecule DZP. More analysis of this region revealed that important interacting residues of binding pocket, i.e., Trp86 and Asp74 interact with all six ligands. This stabilization of higher RMSF value may be due to the interaction of aforementioned residues with ligands.

3.2.4. Solvent accessibility surface area and hydrogen bond analysis

The percentage change in SASA of the residues presents 10 Å away from the ligands was calculated. It was found that there was a considerable decrease in SASA of active site residues of AChE in the presence of all ligands. Figure 9(A) represents the percentage decrease in SASA of AChE in the presence of different ligands with respect to simulation time. Figure 9(B) shows the average percentage decrease in SASA

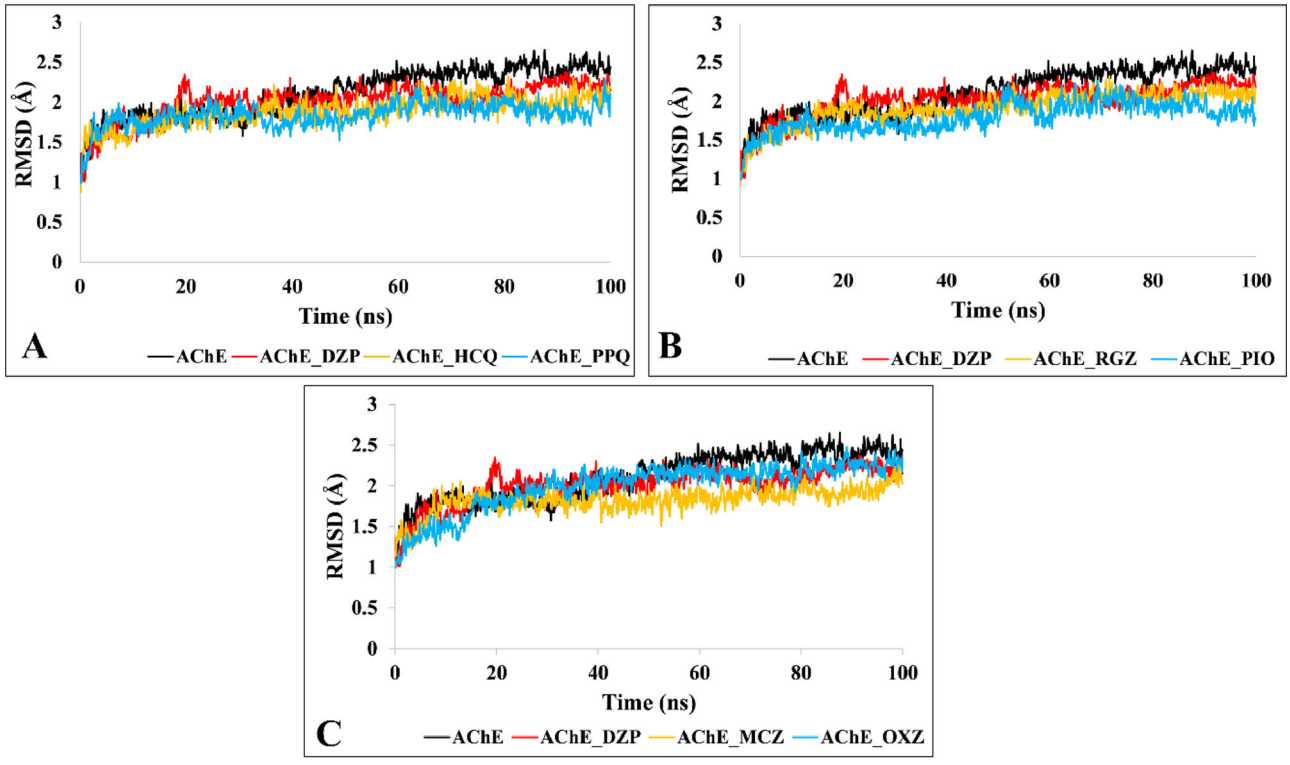

Figure 7. Backbone RMSD plot for apo-AChE and AChE–donepezil complex in comparison with (A) AChE-HCQ, AChE-PPQ; (B) AChE-RGZ, AChE-PIO; and (C) AChE-MCZ, AChE-OXZ with respect to simulation time.

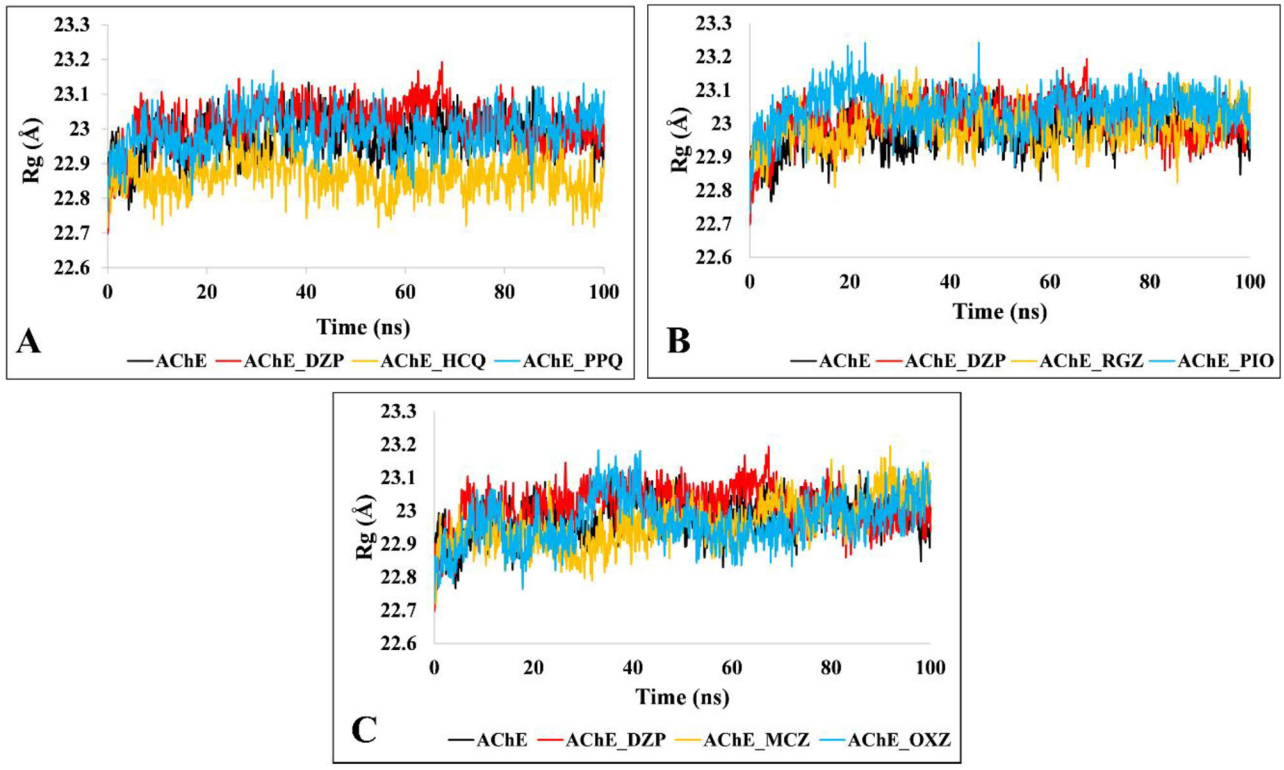

Figure 8. The radius of gyration plot for apo-AChE and AChE–donepezil complex in comparison with (A) AChE-HCQ, AChE-PPQ; (B) AChE-RGZ, AChE-PIO; and (C) AChE-MCZ, AChE-OXZ with respect to simulation time.

of AChE residues 10 Å away from ligands. It can be concluded from this analysis that there was approximately 20%–25% decrease in SASA of active site residues of AChE in the presence of all ligands. Supplementary Figure S8 also represents the SASA value fluctuations of whole protein in the presence of ligands with respect to simulation time. The majority of changes in SASA values occur in the active site residues.

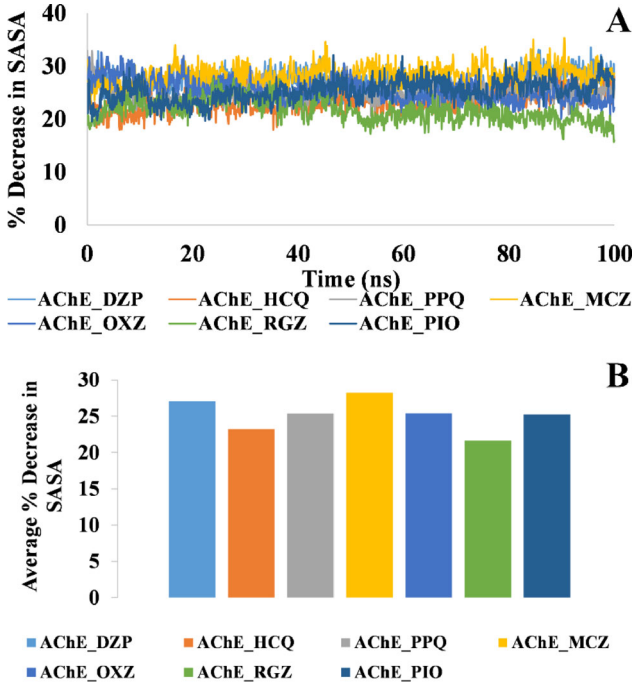

Figure 9. (A) Percentage decrease in SASA of active site residues (10 Å away from the bound ligand) with respect to simulation time in the presence of different ligands; (B) average percentage decrease in SASA of active site residues of AChE calculated from 1000 snapshots obtained from MD simulations.

Table 3. *h*AChE inhibition by hydroxychloroquine, rosiglitazone and donepezil.

Compound	IC_{50} ± SEM (μM)
Hydroxychloroquine	9.64 ± 0.19
Rosiglitazone	13.10 ± 0.18
Donepezil	0.086 ± 0.12

The number of hydrogen bonds formed between the AChE and all seven ligands was calculated. The plots in Supplementary Figures S9 and S10 depict the total number of hydrogen bonds a particular ligand makes with AChE with respect to simulation time. The detailed histogram analysis (Supplementary Figure S11) obtained from the simulation data shows that most of the time DZP makes only one hydrogen bond with AChE. Similarly, azole family drug molecules, i.e., MCZ makes no hydrogen bonds while OXZ makes one hydrogen bond with active residues of AChE (Supplementary Figure S12). The HCQ and PPQ mostly make two hydrogen bonds with AChE during the simulation (Supplementary Figure S11).

3.3. In vitro hAChE inhibition assays

In clinical practice, it is well known that ChE inhibitors are an effective approach in improving the cognitive decline in AD. Thus, the inhibitory activities of the compounds (HCQ and RGZ) on *h*AChE were measured according to the modified Ellman method (Ellman et al., 1961) and following previous publications (Kumar, Ganeshpurkar, et al., 2018; Kumar, Gupta, et al., 2018; Singh et al., 2020). DZP, a well-known cholinesterase inhibitor available in the market for AD, was used as a reference drug. The tested target compounds exhibited mild-to-moderate inhibitory activity against *h*AChE

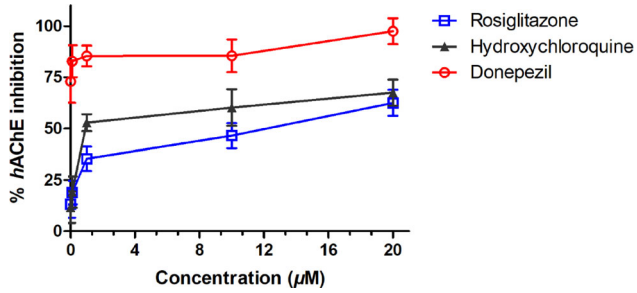

Figure 10. Percentage inhibition of *h*AChE by rosiglitazone, hydroxychloroquine and donepezil.

with IC_{50} values in the range of μM concentration (Table 3). However, in comparison to DZP, the enzyme inhibition property was found to be weak for the tested molecules. The IC_{50} values and percentage inhibition graph for *h*AChE inhibition are summarized in Table 3 and Figure 10. As shown in Table 3, RGZ and HCQ could inhibit *h*AChE with IC_{50} = 13.10 ± 0.18 μM and 9.64 ± 0.19 μM, respectively.

4. Discussion

In this study, FDA-approved drugs were computationally screened using a combined three-stage VS protocol which includes molecular docking, binding free energy calculation and BBB prediction. It leads to the identification of 22 hits out of a total of 2389 molecules. Literature search was performed on top 10 hits and it leads to the identification of six drug molecules (refer to Section 3.1). This includes HCQ, RGZ and PIO, which have been already shown to have beneficial effects in mild-to-moderate AD in animal models and patients (Aisen, 2002; Aisen et al., 2001; Pedersen et al., 2006; Pérez & Quintanilla, 2015). The antifungal drug MCZ has been already shown to have AChE inhibitory activity and efforts have been made to design new potent derivatives using the MCZ scaffold (Chen et al., 2015). The remaining two drug molecules PPQ and OXZ share structural similarity with HCQ and MCZ, respectively, and also have ranked higher in *in silico* study. The RMSD, R_g and RMSF analysis shows that protein–ligand complexes were stable during MD simulations. MD simulation study also reveals the information about important interacting residues of PAS (Asp74, Tyr124 and Trp286) and catalytic active site residues (Trp86, Glu202 and Tyr337) of *h*AChE with different ligands. All these six final selected hits belong to three main classes, i.e., antidiabetic, antimalarial and antifungal. We focused on *in vitro* *h*AChE inhibition assay on a single drug from each class to reduce experimental cost. Later, antifungal class compounds were excluded as the *h*AChE inhibitory activity of MCZ was already reported in the literature. Finally, RGZ and HCQ were tested against the *h*AChE enzyme and found that they could inhibit the enzyme with IC_{50} values 13.10 ± 0.18 and 9.64 ± 0.19 μM, respectively. This indicated the moderate interaction of these molecules with the target as compared to standard potent molecule DZP. Our study also shows that all six molecules despite being classified into three different classes, i.e., TZD (T2DM class), aminoquinoline (antimalarial) and azoles (antifungal), have a tertiary amine as a common

pharmacophoric feature present in all molecules (Supplementary Figure S13). This chemical feature was also found to be present in other already well-established and marketed AChE inhibitors like DZP, rivastigmine, galantamine and physostigmine.

The detailed computational insights from docking and simulation data may shed light on the possible reason behind the large difference in IC_{50} value between highly potent DZP and less potent molecules RGZ and HCQ. The MD simulation of docked AChE-DZP complex reveals the critical and important interaction with the key residues of AChE. It was observed that the DZP interacts with two critical residues, i.e., Trp86 and Trp286 of *h*AChE through hydrophobic interaction (i.e. π–π stacking and π–cation interaction) during the simulation. The residue Trp86 belongs to the CAS portion, whereas the Trp286 belongs to the PAS portion of the *h*AChE binding pocket, and DZP interacts efficiently with both residues. While this kind of concomitant synergy via the hydrophobic interaction to Trp of both PAS and CAS was absent in case of RGZ and PIO. Another possible important difference was that the docking score of RGZ and PIO was −9.57 and −12.04 kcal/mol, which is quite high as compared to the docking score of DZP, i.e., −17.48 kcal/mol. Hence, the measured mid-range μM level AChE inhibition by RGZ and HCQ may be explained by the aforementioned observation concluded from the computational study.

The emerging evidence suggests an association between AD and type 2 diabetes mellitus; which may contribute to one another's pathophysiology and clinical symptoms. It has been demonstrated that the presence of insulin-sensitive glucose transporters and insulin receptors in the medial temporal regions of the brain are necessary to perform the normal cognitive function. Thus, insulin abnormality can deteriorate memory function and cause Alzheimer-like clinical symptoms (Craft & Watson, 2004; Watson & Craft, 2003). Craft in 2007 suggested that a rise in plasma insulin in the insulin resistance individuals increases the level of β-amyloid (Aβ) and other inflammatory agents in the brain (Craft, 2007). Therefore, consistent efforts have been made to repurpose the TZD class of antidiabetic drugs against AD owing to their potent insulin-sensitizing action through the PPAR-γ. However, experimental and clinical data available related to RGZ and PIO drugs showed limited success against the AD (Geldmacher et al., 2011; Risner et al., 2006; Watson et al., 2005). Escribano et al. in 2009 used mice overexpressing mutant human amyloid precursor protein to understand the mechanism of RGZ in the improvement of cognitive function in AD and has indicated the possible involvement of glucocorticoid receptor (GR) (Escribano et al., 2009). Similarly, Moreira in 2018 highlighted mitochondrial dysfunction as a link between both the diseases and suggested that TZD increases mitochondrial biogenesis in human adipose tissue and neuronal NT2 cells, which further help in the modulation of disease pathophysiology (Moreira, 2018). All of the aforementioned mechanism explains the mechanistic viewpoint for the possible beneficial effect of TZD in AD but it did not establish any link between TZDs and cholinergic hypothesis of AD. But here our study shows that RGZ inhibits *h*AChE which is not yet reported in the literature. However, Harrington et al. in 2011 used RGZ as adjunctive therapy with potent AChE inhibitors and found no significant effect on individuals (Harrington et al., 2011). It might be due to the fact that RGZ had to compete with potent AChE inhibitors and therefore, no significant effects were seen. Hence our preliminary research indicates that more experimental study is needed to establish any possible link between AChE inhibition of TZD and its beneficial role in AD.

HCQ is another drug that has been reported to show beneficial effects in AD patients by its ability to inhibit the destructive inflammatory mechanisms. The AChE inhibition activity of aminoquinoline derivatives, i.e., chloroquine, amodiaquine, amopyroquine and primaquine is already reported in the literature except for HCQ (Katewa & Katyare, 2005; Lim & Go, 1985). However, HCQ was found to inhibit the butyrylcholinesterase with IC_{50} value of 0.38 ± 1.4 μM in a study (Dawson et al., 2005). Here, through this study, we report that HCQ also inhibits the *h*AChE and this suggests that apart from the anti-inflammatory effect of HCQ, the moderate inhibition of AChE may also have some role in showing the beneficial effect in the AD. Our study suggests the possible impact of HCQ on the cholinergic pathway, which is one of the key players in AD. However, a study performed by van Gool et al. in 2001 observed no significant effect in early-stage Alzheimer's patients in a double-blind trial using HCQ (van Gool et al., 2001). Several reasons can explain why these drugs (RGZ, PIO and HCQ) which have AChE inhibitory activity but cannot produce clear cut significant effect among individuals. The high IC_{50} value of these molecules in comparison to DZP may be one of the possible reasons behind the mixed effect observed in clinical trials for AD patients.

In conclusion, the current drug repurposing study using the computational method supplemented by experimental enzyme assay confirms AChE inhibitory activity of HCQ and RGZ. These new findings on TZD and aminoquinoline class of drugs and its role in AD may open up new possibilities in drug repurposing for AD. The detailed computational information about the AChE inhibitory activity of antifungal azoles class of drug (MCZ and OXZ) can be used to design more potent AChE inhibitors. The study also reveals detailed computational insights on stability of protein–ligand complex, information about critical interacting residues, orientation of drug molecules in pockets and average binding free energy through long MD simulation study.

Acknowledgment

The authors acknowledge Director, Prof. Maitreyee Dutta and Prof. K. G. Srinivasa of NITTTR, Chandigarh for providing computational infrastructure. Y.P.S. is thankful to Indian Institute of Technology (BHU) and MHRD, India for fellowship.

Disclosure statement

No potential conflict of interest was reported by the authors.

Funding

The biological assay was performed at IIT BHU and supported by Science and Engineering Research Board under Core Research Grant (SERB-CRG/2018/003490) and Indian Institute of Technology (BHU) (SM/2016-17/1198/L).

ORCID

Navneet Kumar http://orcid.org/0000-0003-4104-5187

References

Aisen, P. S. (2002). The potential of anti-inflammatory drugs for the treatment of Alzheimer's disease. *The Lancet Neurology*, *1*(5), 279–284.

Aisen, P. S., Marin, D. B., Brickman, A. M., Santoro, J., & Fusco, M. (2001). Pilot tolerability studies of hydroxychloroquine and colchicine in Alzheimer disease. *Alzheimer Disease and Associated Disorders*, *15*(2), 96–101. https://doi.org/10.1097/00002093-200104000-00009

Al-Bari, M. A. A. (2015). Chloroquine analogues in drug discovery: New directions of uses, mechanisms of actions and toxic manifestations from malaria to multifarious diseases. *The Journal of Antimicrobial Chemotherapy*, *70*(6), 1608–1621. https://doi.org/10.1093/jac/dkv018

Arora, M., Ganugula, R., Kumar, N., Kaur, G., Pellois, J.-P., Garg, P., & Ravi Kumar, M. (2019). Next-generation noncompetitive nanosystems based on gambogic acid: *In silico* identification of transferrin receptor binding sites, regulatory shelf stability, and their preliminary safety in healthy rodents. *ACS Applied Bio Materials*, *2*(8), 3540–3550. https://doi.org/10.1021/acsabm.9b00419

Ayton, S., Lei, P., & Bush, A. I. (2015). Biometals and their therapeutic implications in Alzheimer's disease. *Neurotherapeutics*, *12*(1), 109–120.

Bansode, S. B., Jana, A. K., Batkulwar, K. B., Warkad, S. D., Joshi, R. S., Sengupta, N., & Kulkarni, M. J. (2014). Molecular investigations of protriptyline as a multi-target directed ligand in Alzheimer's disease. *PLoS One*, *9*(8), e105196.

Berman, H., Westbrook, J., Feng, Z., Gilliland, G., Bhat, T., Weissig, H., Shindyalov, I., Bourne, P., Rose, P., & Prlic, A. (2000). RCSB Protein Data Bank: Structural biology views for basic and applied research. *Nucleic Acids Research*, *28*(1), 235–242. https://doi.org/10.1093/nar/28.1.235

Bibi, N., Rizvi, S., Batool, A., & Kamal, M. A. (2019). Inhibitory mechanism of an anticancer drug, bexarotene against amyloid β peptide aggregation: Repurposing via neuroinformatics approach. *Current Pharmaceutical Design*, *25*(27), 2989–2995. https://doi.org/10.2174/1381612825666190801123235

Bowers, K. J., Chow, D. E., Xu, H., Dror, R. O., Eastwood, M. P., Gregersen, B. A., Klepeis, J. L., Kolossvary, I., Moraes, M. A., Sacerdoti, F. D. (2006). *Scalable algorithms for molecular dynamics simulations on commodity clusters* [Paper presentation]. SC'06: Proceedings of the 2006 ACM/IEEE Conference on Supercomputing, Tampa, FL, USA, November 11–17.

Burns, A., & Iliffe, S. (2009). Alzheimer's disease. *BMJ 338*, b158. https://doi.org/10.1136/bmj.b158

Castro, A., & Martinez, A. (2006). Targeting beta-amyloid pathogenesis through acetylcholinesterase inhibitors. *Current Pharmaceutical Design*, *12*(33), 4377–4387. https://doi.org/10.2174/138161206778792985

Chen, Y., Xu, X., Fu, T., Li, W., Liu, Z., & Sun, H. (2015). Discovery of new scaffolds from approved drugs as acetylcholinesterase inhibitors. *RSC Advances*, *5*(110), 90288–90294.

Cheung, J., Rudolph, M. J., Burshteyn, F., Cassidy, M. S., Gary, E. N., Love, J., Franklin, M. C., & Height, J. J. (2012). Structures of human acetylcholinesterase in complex with pharmacologically important ligands. *Journal of Medicinal Chemistry*, *55*(22), 10282–10286. https://doi.org/10.1021/jm300871x

Cho, K., Joannopoulos, J., & Kleinman, L. (1993). Constant-temperature molecular dynamics with momentum conservation. *Physical review. E, Statistical Physics, Plasmas, Fluids, and Related Interdisciplinary Topics*, *47*(5), 3145–3151. https://doi.org/10.1103/physreve.47.3145

Colovic, M. B., Krstic, D. Z., Lazarevic-Pasti, T. D., Bondzic, A. M., & Vasic, V. M. (2013). Acetylcholinesterase inhibitors: Pharmacology and toxicology. *Current Neuropharmacology*, *11*(3), 315–335.

Craft, S. (2007). Insulin resistance and Alzheimer's disease pathogenesis: Potential mechanisms and implications for treatment. *Current Alzheimer Research*, *4*(2), 147–152. https://doi.org/10.2174/156720507780362137

Craft, S., & Watson, G. S. (2004). Insulin and neurodegenerative disease: Shared and specific mechanisms. *The Lancet Neurology*, *3*(3), 169–178.

Dawson, L., Caulfield, V., Stanbury, J., Field, A., Christmas, S., & Smith, P. (2005). Hydroxychloroquine therapy in patients with primary Sjögren's syndrome may improve salivary gland hypofunction by inhibition of glandular cholinesterase. *Rheumatology*, *44*(4), 449–455.

Dong, Y.-F., Kataoka, K., Tokutomi, Y., Nako, H., Nakamura, T., Toyama, K., Sueta, D., Koibuchi, N., Yamamoto, E., Ogawa, H., & Kim-Mitsuyama, S. (2011). Perindopril, a centrally active angiotensin-converting enzyme inhibitor, prevents cognitive impairment in mouse models of Alzheimer's disease. *FASEB Journal*, *25*(9), 2911–2920. https://doi.org/10.1096/fj.11-182873

Egan, W. J., & Lauri, G. (2002). Prediction of intestinal permeability. *Advanced Drug Delivery Reviews*, *54*(3), 273–289.

Ellman, G. L., Courtney, K. D., Andres, V., & Feather-Stone, R. M. (1961). A new and rapid colorimetric determination of acetylcholinesterase activity. *Biochemical Pharmacology*, *7*, 88–95.

Escribano, L., Simón, A.-M., Pérez-Mediavilla, A., Salazar-Colocho, P., Del Río, J., & Frechilla, D. (2009). Rosiglitazone reverses memory decline and hippocampal glucocorticoid receptor down-regulation in an Alzheimer's disease mouse model. *Biochemical and Biophysical Research Communications*, *379*(2), 406–410. https://doi.org/10.1016/j.bbrc.2008.12.071

Evans, D. J., & Holian, B. L. (1985). The Nose–Hoover thermostat. *The Journal of Chemical Physics*, *83*(8), 4069–4074.

Forloni, G., Colombo, L., Girola, L., Tagliavini, F., & Salmona, M. (2001). Anti-amyloidogenic activity of tetracyclines: Studies in vitro. *FEBS Letters*, *487*, 404–407.

Francis, P. T., Palmer, A. M., Snape, M., & Wilcock, G. K. (1999). The cholinergic hypothesis of Alzheimer's disease: A review of progress. *Journal of Neurology, Neurosurgery, and Psychiatry*, *66*(2), 137–147. https://doi.org/10.1136/jnnp.66.2.137

Friesner, R. A., Murphy, R. B., Repasky, M. P., Frye, L. L., Greenwood, J. R., Halgren, T. A., Sanschagrin, P. C., & Mainz, D. T. (2006). Extra precision glide: Docking and scoring incorporating a model of hydrophobic enclosure for protein-ligand complexes. *Journal of Medicinal Chemistry*, *49*(21), 6177–6196. https://doi.org/10.1021/jm051256o

Gauthier, S., Scheltens, P., & Cummings, J. (2005). *Alzheimer's disease and related disorders*. CRC Press.

Gautret, P., Lagier, J.-C., Parola, P., Hoang, V. T., Meddeb, L., Mailhe, M., Doudier, B., Courjon, J., Giordanengo, V., Vieira, V. E., Tissot Dupont, H., Honoré, S., Colson, P., Chabrière, E., La Scola, B., Rolain, J.-M., Brouqui, P., & Raoult, D. (2020). Hydroxychloroquine and azithromycin as a treatment of COVID-19: Results of an open-label non-randomized clinical trial. *International Journal of Antimicrobial Agents*, *56*(1), 105949.

Geldmacher, D. S., Fritsch, T., McClendon, M. J., & Landreth, G. (2011). A randomized pilot clinical trial of the safety of pioglitazone in treatment of patients with Alzheimer disease. *Archives of Neurology*, *68*(1), 45–50. https://doi.org/10.1001/archneurol.2010.229

Genheden, S., & Ryde, U. (2015). The MM/PBSA and MM/GBSA methods to estimate ligand-binding affinities. *Expert Opinion on Drug Discovery*, *10*(5), 449–461. https://doi.org/10.1517/17460441.2015.1032936

Grundke-Iqbal, I., Iqbal, K., Tung, Y.-C., Quinlan, M., Wisniewski, H. M., & Binder, L. I. (1986). Abnormal phosphorylation of the microtubule-associated protein tau (tau) in Alzheimer cytoskeletal pathology. *Proceedings of the National Academy of Sciences of the United States of America*, *83*(13), 4913–4917. https://doi.org/10.1073/pnas.83.13.4913

Harrington, C., Sawchak, S., Chiang, C., Davies, J., Donovan, C., Saunders, A. M., Irizarry, M., Jeter, B., Zvartau-Hind, M., van Dyck, C. H., & Gold, M. (2011). Rosiglitazone does not improve cognition or global function when used as adjunctive therapy to AChE inhibitors in mild-to-

moderate Alzheimer's disease: Two phase 3 studies. *Current Alzheimer Research*, *8*(5), 592–606. https://doi.org/10.2174/156720511796391935

Hayes, C. D., Dey, D., Palavicini, J. P., Wang, H., Patkar, K. A., Minond, D., Nefzi, A., & Lakshmana, M. K. (2013). Striking reduction of amyloid plaque burden in an Alzheimer's mouse model after chronic administration of carmustine. *BMC Medicine*, *11*(1), 81.

Holzgrabe, U., Kapková, P., Alptüzün, V., Scheiber, J., & Kugelmann, E. (2007). Targeting acetylcholinesterase to treat neurodegeneration. *Expert Opinion on Therapeutic Targets*, *11*(2), 161–179. https://doi.org/10.1517/14728222.11.2.161

Hoover, W. G. (1985). Canonical dynamics: Equilibrium phase-space distributions. *Physical Review. A: General Physics*, *31*(3), 1695–1697. https://doi.org/10.1103/physreva.31.1695

Hughes, R. E., Nikolic, K., & Ramsay, R. R. (2016). One for all? Hitting multiple Alzheimer's disease targets with one drug. *Frontiers in Neuroscience*, *10*, 177. https://doi.org/10.3389/fnins.2016.00177

Junaid, M., Islam, N., Hossain, M. K., Ullah, M. O., & Halim, M. A. (2019). Metal based donepezil analogues designed to inhibit human acetylcholinesterase for Alzheimer's disease. *PLoS One*, *14*(2), e0211935.

Karaman, B., & Sippl, W. (2019). Computational drug repurposing: Current trends. *Current Medicinal Chemistry*, *26*(28), 5389–5409. https://doi.org/10.2174/0929867325666180530100332

Katewa, S. D., & Katyare, S. S. (2005). Antimalarials inhibit human erythrocyte membrane acetylcholinesterase. *Drug and Chemical Toxicology*, *28*(4), 467–482. https://doi.org/10.1080/01480540500262912

Kumar, S., Chowdhury, S., & Kumar, S. (2017). *In silico* repurposing of antipsychotic drugs for Alzheimer's disease. *BMC Neuroscience*, *18*(1), 76. https://doi.org/10.1186/s12868-017-0394-8

Kumar, D., Ganeshpurkar, A., Kumar, D., Modi, G., Gupta, S. K., & Singh, S. K. (2018). Secretase inhibitors for the treatment of Alzheimer's disease: Long road ahead. *European Journal of Medicinal Chemistry*, *148*, 436–452. https://doi.org/10.1016/j.ejmech.2018.02.035

Kumar, D., Gupta, S. K., Ganeshpurkar, A., Gutti, G., Krishnamurthy, S., Modi, G., & Singh, S. K. (2018). Development of piperazinediones as dual inhibitor for treatment of Alzheimer's disease. *European Journal of Medicinal Chemistry*, *150*, 87–101. https://doi.org/10.1016/j.ejmech.2018.02.078

Lim, L., & Go, M. (1985). The anticholinesterase activity of mefloquine. *Clinical and Experimental Pharmacology and Physiology*, *12*(5), 527–531. https://doi.org/10.1111/j.1440-1681.1985.tb00904.x

Lyne, P. D., Lamb, M. L., & Saeh, J. C. (2006). Accurate prediction of the relative potencies of members of a series of kinase inhibitors using molecular docking and MM-GBSA scoring. *Journal of Medicinal Chemistry*, *49*(16), 4805–4808. https://doi.org/10.1021/jm060522a

Mark, P., & Nilsson, L. (2001). Structure and dynamics of the TIP3P, SPC, and SPC/E water models at 298 K. *The Journal of Physical Chemistry A*, *105*, 9954–9960.

Mayeux, R., & Stern, Y. (2012). Epidemiology of Alzheimer disease. *Cold Spring Harbor Perspectives in Medicine*, *2*(8), a006239.

McGleenon, B., Dynan, K., & Passmore, A. (1999). Acetylcholinesterase inhibitors in Alzheimer's disease. *British Journal of Clinical Pharmacology*, *48*(4), 471–480. https://doi.org/10.1046/j.1365-2125.1999.00026.x

Mehta, M., Adem, A., & Sabbagh, M. (2012). New acetylcholinesterase inhibitors for Alzheimer's disease. *International Journal of Alzheimer's Disease*, *2012*, 728983.

Méndez-Lucio, O., Tran, J., Medina-Franco, J. L., Meurice, N., & Muller, M. (2014). Toward drug repurposing in epigenetics: Olsalazine as a hypomethylating compound active in a cellular context. *ChemMedChem*, *9*(3), 560–565. https://doi.org/10.1002/cmdc.201300555

Meulenbroek, O., O'Dwyer, S., de Jong, D., van Spijker, G., Kennelly, S., Cregg, F., Olde Rikkert, M., Abdullah, L., Wallin, A., Walsh, C., Coen, R., Kenny, R. A., Daly, L., Segurado, R., Borjesson-Hanson, A., Crawford, F., Mullan, M., Lucca, U., Banzi, R., … Lawlor, B. (2016). European multicentre double-blind placebo-controlled trial of Nilvadipine in mild-to-moderate Alzheimer's disease—The substudy protocols: NILVAD frailty; NILVAD blood and genetic biomarkers; NILVAD cerebrospinal fluid biomarkers; NILVAD cerebral blood flow. *BMJ Open*, *6*(7), e011584.

Miller, B. W., Willett, K. C., & Desilets, A. R. (2011). Rosiglitazone and pioglitazone for the treatment of Alzheimer's disease. *The Annals of Pharmacotherapy*, *45*(11), 1416–1424. https://doi.org/10.1345/aph.1Q238

Moreira, P. I. (2018). Sweet mitochondria: A shortcut to Alzheimer's disease. *Journal of Alzheimer's Disease*, *62*(3), 1391–1401. https://doi.org/10.3233/JAD-170931

Naveja, J. J., Dueñas-González, A., & Medina-Franco, J. L. (2016). Drug repurposing for epigenetic targets guided by computational methods. In J. L. Medina-Franco (Ed.), Epi-informatics (pp. 327–357). Elsevier.

Nosé, S. (1984). A unified formulation of the constant temperature molecular dynamics methods. *The Journal of Chemical Physics*, *81*(1), 511–519.

Pedersen, W. A., McMillan, P. J., Kulstad, J. J., Leverenz, J. B., Craft, S., & Haynatzki, G. R. (2006). Rosiglitazone attenuates learning and memory deficits in Tg2576 Alzheimer mice. *Experimental Neurology*, *199*(2), 265–273. https://doi.org/10.1016/j.expneurol.2006.01.018

Pérez, M. J., & Quintanilla, R. A. (2015). Therapeutic actions of the thiazolidinediones in Alzheimer's disease. *PPAR Research*, *2015*, 957248.

Pushpakom, S., Iorio, F., Eyers, P. A., Escott, K. J., Hopper, S., Wells, A., Doig, A., Guilliams, T., Latimer, J., McNamee, C., Norris, A., Sanseau, P., Cavalla, D., & Pirmohamed, M. (2019). Drug repurposing: Progress, challenges and recommendations. *Nature Reviews. Drug Discovery*, *18*(1), 41–58. https://doi.org/10.1038/nrd.2018.168

Raja, S. G., & Nayak, S. H. (2004). Sildenafil: Emerging cardiovascular indications. *The Annals of Thoracic Surgery*, *78*(4), 1496–1506. https://doi.org/10.1016/j.athoracsur.2004.02.125

Risner, M., Saunders, A., Altman, J., Ormandy, G., Craft, S., Foley, I., Zvartau-Hind, M., Hosford, D., & Roses, A., & Rosiglitazone in Alzheimer's Disease Study Group. (2006). Efficacy of rosiglitazone in a genetically defined population with mild-to-moderate Alzheimer's disease. *The Pharmacogenomics Journal*, *6*(4), 246–254. https://doi.org/10.1038/sj.tpj.6500369

Ryu, J. K., Franciosi, S., Sattayaprasert, P., Kim, S. U., & McLarnon, J. G. (2004). Minocycline inhibits neuronal death and glial activation induced by β-amyloid peptide in rat hippocampus. *Glia*, *48*(1), 85–90. https://doi.org/10.1002/glia.20051

Samad, F. A., Suliman, B. A., Basha, S. H., Manivasagam, T., & Essa, M. M. (2016). A comprehensive *in silico* analysis on the structural and functional impact of SNPs in the congenital heart defects associated with NKX2-5 gene—A molecular dynamic simulation approach. *PLoS One*, *11*(5), e0153999.

Sanchez, P. E., Zhu, L., Verret, L., Vossel, K. A., Orr, A. G., Cirrito, J. R., Devidze, N., Ho, K., Yu, G.-Q., Palop, J. J., & Mucke, L. (2012). Levetiracetam suppresses neuronal network dysfunction and reverses synaptic and cognitive deficits in an Alzheimer's disease model. *Proceedings of the National Academy of Sciences of the United States of America*, *109*(42), E2895–E2903. https://doi.org/10.1073/pnas.1121081109

Santos, T. C. d., Gomes, T. M., Pinto, B. A. S., Camara, A. L., & Paes, A. M. d. A. (2018). Naturally occurring acetylcholinesterase inhibitors and their potential use for Alzheimer's disease therapy. *Frontiers in Pharmacology*, *9*, 1192. https://doi.org/10.3389/fphar.2018.01192

Scarpini, E., Schelterns, P., & Feldman, H. (2003). Treatment of Alzheimer's disease: Current status and new perspectives. *The Lancet Neurology*, *2*(9), 539–547.

Shivakumar, D., Williams, J., Wu, Y., Damm, W., Shelley, J., & Sherman, W. (2010). Prediction of absolute solvation free energies using molecular dynamics free energy perturbation and the OPLS force field. *Journal of Chemical Theory and Computation*, *6*(5), 1509–1519. https://doi.org/10.1021/ct900587b

Singh, Y. P., Pandey, A., Vishwakarma, S., & Modi, G. (2019). A review on iron chelators as potential therapeutic agents for the treatment of Alzheimer's and Parkinson's diseases. *Molecular Diversity*, *23*(2), 509–526. https://doi.org/10.1007/s11030-018-9878-4

Singh, B., Sharma, B., Jaggi, A. S., & Singh, N. (2013). Attenuating effect of lisinopril and telmisartan in intracerebroventricular streptozotocin induced experimental dementia of Alzheimer's disease type: Possible involvement of PPAR-γ agonistic property. *Journal of the Renin-*

Angiotensin-Aldosterone System, *14*(2), 124–136. https://doi.org/10.1177/1470320312459977

Singh, Y. P., Tej, G. N. V. C., Pandey, A., Priya, K., Pandey, P., Shankar, G., Nayak, P. K., Rai, G., Chittiboyina, A. G., Doerksen, R. J., Vishwakarma, S., & Modi, G. (2020). Design, synthesis and biological evaluation of novel naturally-inspired multifunctional molecules for the management of Alzheimer's disease. *European Journal of Medicinal Chemistry*, *198*, 112257. https://doi.org/10.1016/j.ejmech.2020.112257

Talevi, A., & Bellera, C. L. (2020). Challenges and opportunities with drug repurposing: Finding strategies to find alternative uses of therapeutics. *Expert Opinion on Drug Discovery*, *15*, 397–401. https://doi.org/10.1080/17460441.2020.1704729

Tariot, P. N., Schneider, L. S., Cummings, J., Thomas, R. G., Raman, R., Jakimovich, L. J., Loy, R., Bartocci, B., Fleisher, A., & Ismail, M. S. (2011). Chronic divalproex sodium to attenuate agitation and clinical progression of Alzheimer disease. *Archives of General Psychiatry*, *68*(8), 853–861.

van Gool, W. A., Weinstein, H. C., Scheltens, P. K., & Walstra, G. J. (2001). Effect of hydroxychloroquine on progression of dementia in early Alzheimer's disease: An 18-month randomised, double-blind, placebo-controlled study. *The Lancet*, *358*, 455–460.

Watson, G. S., Cholerton, B. A., Reger, M. A., Baker, L. D., Plymate, S. R., Asthana, S., Fishel, M. A., Kulstad, J. J., Green, P. S., Cook, D. G., Kahn, S. E., Keeling, M. L., & Craft, S. (2005). Preserved cognition in patients with early Alzheimer disease and amnestic mild cognitive impairment during treatment with rosiglitazone: A preliminary study. *The American Journal of Geriatric Psychiatry*, *13*(11), 950–958.

Watson, G. S., & Craft, S. (2003). The role of insulin resistance in the pathogenesis of Alzheimer's disease: Implications for treatment. *CNS Drugs*, *17*(1), 27–45. https://doi.org/10.2165/00023210-200317010-00003

Wishart, D. S., Knox, C., Guo, A. C., Cheng, D., Shrivastava, S., Tzur, D., Gautam, B., & Hassanali, M. (2008). DrugBank: A knowledgebase for drugs, drug actions and drug targets. *Nucleic Acids Research*, *36*(Database issue), D901–D906. https://doi.org/10.1093/nar/gkm958

Zhang, L., Li, D., Cao, F., Xiao, W., Zhao, L., Ding, G., & Wang, Z. Z. (2018). Identification of human acetylcholinesterase inhibitors from the constituents of EGb761 by modeling docking and molecular dynamics simulations. *Combinatorial Chemistry & High Throughput Screening*, *21*(1), 41–49. https://doi.org/10.2174/1386207320666171123201910